A highly active and synergistic $Pt/Mo_2C/Al_2O_3$ catalysts for Water-Gas Shift Reaction

Ahmed I. Osman [a, b*], Jehad K. Abu-Dahrieh[a]*, Nikolay Cherkasov[c], Javier Fernandez-Garcia[c], David Walker[d], Richard I. Walton[e], David W. Rooney[a], Evgeny Rebrov[c,f]

[a] School of Chemistry and Chemical Engineering, Queen's University Belfast, Belfast BT9 5AG, Northern Ireland, UK

[b] Chemistry Department, Faculty of Science-Qena, South Valley University, Qena 83523, Egypt.

[c] School of Engineering, University of Warwick, Coventry, CV4 7AL, UK

[d] Department of Physics, University of Warwick, Coventry, CV4 7AL, UK

[e] Department of Chemistry, University of Warwick, Coventry, CV4 7AL, UK

[f] Department of Biotechnology and Chemistry, Tver State Technical University, Russia

ORCID information

Ahmed I. Osman: http://orcid.org/0000-0003-2788-7839

Evgeny Rebrov: http://orcid.org/0000-0001-6056-9520

Richard Walton: https://orcid.org/0000-0001-9706-2774

David W. Rooney: https://orcid.org/0000-0001-5036-2497

Nikolay Cherkasov: https://orcid.org/0000-0001-5979-8713

Corresponding Author: Ahmed I. Osman, Jehad Abu-Dahrieh

Email: aosmanahmed01@qub.ac.uk, j.abudahrieh@qub.ac.uk

Address: School of Chemistry and Chemical Engineering, Queen's University Belfast, David Keir Building, Stranmillis Road, Belfast BT9 5AG, Northern Ireland, United Kingdom

Fax: +44 2890 97 4687

Tel.: +44 2890 97 4269

Abstract

Catalysts consisting of Pt and Cu supported on Mo_2C/η-Al_2O_3, Mo_2C/γ-Al_2O_3 or Mo_2C were prepared and used for the low-temperature water gas shift reaction. The catalysts were characterized by elemental analysis, X-ray diffraction (XRD), temperature-programmed reduction (TPR), X-ray photoelectron spectroscopy (XPS) and scanning electron microscopy (SEM). The catalysts were studied in water gas shift reaction (WGSR) with a reaction mixture containing 11 % CO, 43 % H_2, 6% CO_2, 21 % H_2O (real feed composition mixture from the reformer) and balance He, with a reaction temperature range of 180-300 °C at a space velocity (SV) of 125,000 h^{-1}. Catalyst supports (η-Al_2O_3 and γ-Al_2O_3), led to different synergetic effect between the two most active phases of Pt metal and Mo_2C. Pt/ Mo_2C/η-Al_2O_3 is a promising catalyst (44% conversion at 180°C) due to the close interaction between Pt and Mo_2C phases on the surface of the catalyst. The 4 Pt-Mo_2C showed the highest activity where the temperature at which 50% conversion observed was at only 180 °C with SV of 125,000 h^{-1} and constant stability over 85 hours.

Keywords: Water Gas Shift Reaction; Molybdenum carbide, Platinum, alumina, syngas.

Graphical Abstract

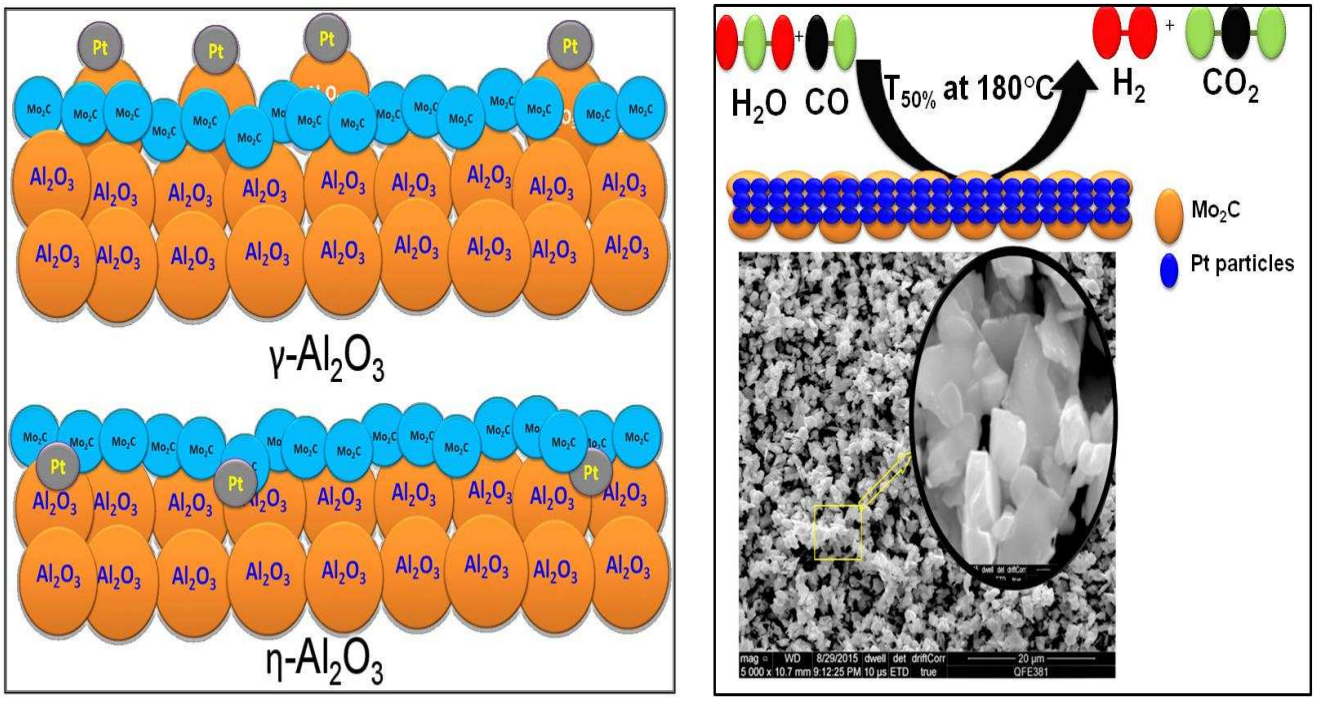

Catalyst composition of $Pt/Mo_2C/Al_2O_3$ WGSR over Pt/Mo_2C catalyst

Research highlights

- Molybdenum carbide is the active phase in water gas shift reaction
- The dispersion of Mo_2C during the carburization was enhanced with Pt
- Pt/Mo_2C catalysts are better than Cu/Mo_2C modified catalysts in WGSR.
- Using different acidic supports affect the synergetic effect between Pt and Mo_2C.
- Pt/Mo_2C showed higher catalytic activity than that of the commercial CuZnAl catalyst

1. Introduction

Nowadays, great attention is paid toward the water gas shift reaction (WGSR) as it offers a way of producing additional H_2 as well as eliminating harmful CO emissions in a variety of industrial applications to meet the safety and environmental requirements. The rise of bio-oil pyrolysis and subsequent methanol production makes a significant use of research into novel water-gas shift catalysts [1, 2]. The reaction feed for WGSR usually comes from of syngas (a mixture of CO and H_2), generated by various processes such as biomass or coal gasification, methane steam or dry reforming, and methane partial oxidation.

At the industrial scale, the WGSR is carried out in two separate steps, high and low-temperature WGSR, to shift the equilibrium of the exothermic reaction into the desired direction. WGSR is used in preparing gases for fuel cells. High-temperature proton exchange membrane (HT-PEM) fuel cells can tolerate CO concentrations up to 3 vol.% [3], however, for low temperature (LT) fuel cells it is necessary to reduce CO concentration to less than 50 ppm for Pt electrode [4]. The drive for the production of synthetic fuels requires novel compact catalysts with a fast start-up time [5].

Noble metals supported onto reducible oxides represent a large class of novel WGSR catalysts. Choung et al.[6] observed a higher WGSR rate over a bimetallic Pt-Re catalyst supported onto a CeO_2-ZrO_2 mixed metal oxide than the rates calculated by addition of individual rates over monometallic Pt and Re catalysts. The simultaneous addition of both Mo and Pt to WGSR catalysts supported on alumina (or silica) increases CO reaction rate at a temperature around 300 ^oC [7] which is related to decreasing CO binding energy over PtMo alloys. However, the authors observed a lower TOF over the bimetallic PtMo supported catalysts compared to Pt/CeO_2 catalyst.

Transition metal carbides such as Mo_2C and Co_2C have been established as active and selective catalysts for the WGSR [4, 8, 9]. Gnanamani et al.[10] studied the WGS reaction over alkali-

promoted Co_2C catalysts. They found that a Na/Co_2C catalyst showed a CO conversion of 76.3% at 240 °C. The authors suggested that the activity of the cobalt-based catalysts is primarily due to the carbide phases and the alkali metals (Na and K) promote catalytic activity by keeping cobalt in the reduced state. An active site density in Mo_2C catalysts is 25% greater than that in a commercial $Cu/ZnO/Al_2O_3$ catalyst. Therefore, the Mo_2C catalysts have a potential to replace the latter in a number of small-scale reactors for WGSR [11]. Thin layers of Mo_2C catalysts supported onto a Mo substrate demonstrate catalytic activity in the WGSR by 1–2 orders of magnitude higher than that of the commercial $Cu/ZnO/Al_2O_3$ catalyst [12, 13]. The catalytic activity of a bulk Mo_2C catalyst can further be improved by 4-5 times after the addition of small amounts of Pt [8]. The reaction rate over a $Pt/Mo_2C/Al_2O_3$ catalyst of 69.2 μmol g_{cat}^{-1} s^{-1} was higher as compared to that of 61.8 μmol g_{cat}^{-1} s^{-1} over a $Cu/Zn/Al_2O_3$ catalyst, while the turnover frequency (TOF) over the $Pt/Mo_2C/Al_2O_3$ catalyst of was reported to be 0.81 s^{-1} [9].

The highest WGSR rate of 284.6 μmol $gcat^{-1}$ s^{-1} was observed at 240 °C over a non-supported Pt/Mo_2C catalyst [9]. The exceptionally high activity of the Pt/Mo_2C catalyst prepared by an aqueous wet impregnation method was due to the high density of active sites and the strong interaction between highly dispersed Pt nanoparticles and the Mo_2C support [4]. A high stability of the Pt/Mo_2C catalyst was also reported in the methanol electro-oxidation which has a similar reaction mechanism [14]. It was observed that Pt (i) increased the stability of Mo_2C support due to a strong chemical interaction and (ii) created a synergetic effect between the Pt nanoparticles and the Mo_2C phase.

We have studied precious metal catalysts [15] and molybdenum carbides [12, 16-19] in the medium temperature range. Among the precious metals, a Pt/Mo_2C catalyst has demonstrated the most promising results [5], with the temperature of 50% conversion (T_{50}%) of 180 °C at a space velocity (SV) of 125,000 h^{-1}. Sabnis et al.[8, 20] studied WGS reaction over a Pt/Mo_2C catalyst and proposed a dual-site reaction mechanism. According to this mechanism, the

catalytic sites are located at the interface between the Mo_2C and the Pt nanoparticles. The Mo_2C phase adsorbs and activates water, while the Pt nanoparticle chemisorbs CO [8].

The present work aims at the development of novel Mo_2C-containing catalysts with higher activity and stability in the WGSR, by the addition of the Pt and Cu nanoparticles. Previously we obtained η-Al_2O_3 and γ-Al_2O_3 with different surface and bulk characteristics from $Al(NO_3)_3$ and $AlCl_3$ precursors, respectively [21, 22]. Herein, the structure-activity relationship over η-Al_2O_3 and γ-Al_2O_3 supported catalysts with different Mo_2C loadings (33, 50 and 66 wt %) has been studied. While the alumina support allows fast scale-up via screen printing [23], the effect of the catalyst precursor is crucial in heterogeneous catalysis due to its effect on metal dispersion and close interaction between the active sites. Sabnis et al.[8], Wang et al.[9] and Schweitzer et al.[4], used an H_2PtCl_6 precursor to prepare their Pt/Mo_2C catalysts. However, it is well known that the catalysts derived from chlorine-containing precursors could be poisoned by chloride ions adsorbed on the metal surface. For example, the methane total oxidation conversion at 300°C over catalysts prepared from a Cl-containing precursor was much lower as compared to the catalysts prepared from chlorine-free precursors [24, 25].

Herein, we prepared a different range of catalysts using noble (Pt) or transition (Cu) metals loaded on Mo_2C/η-Al_2O_3, Mo_2C/γ-Al_2O_3 or Mo_2C for the low-temperature WGSR. Using different acidic supports (η-Al_2O_3 and γ-Al_2O_3) in the catalyst composition, led to different synergetic effect between Pt and Mo_2C. The prepared catalysts were used in WGSR and compared with the commercial catalyst using a real feed composition mixture from the reformer (11 % CO, 43 % H_2, 6% CO_2, 21 % H_2O).

2. Experimental

2.1 Catalyst preparation

The alumina supports (η-alumina and γ-alumina) were prepared as described in our previous work [21, 26-29] using aluminium nitrate or chloride precursor, after the precipitation by ammonia solution and calcination of the precipitate at 550 °C.

The supported Mo_2C/Al_2O_3 catalysts containing 33, 50 and 66 wt. % Mo_2C were prepared by a wet impregnation of the respective alumina supports with a solution containing ammonium molybdate tetrahydrate precursor ($(NH_4)_6Mo_7O_{24} \cdot 4H_2O$; 81-83% as MoO_3,.Alfa Aesar). The mixture was sonicated at 80 °C (200 HT Crest ultrasonic bath), at a 45 kHz frequency for 3 h and resulted in a homogeneous paste. Then the mixture was dried at 120 °C overnight and calcined at 500 °C for 4 h under air with a heating rate of 2 °C min^{-1}. After calcination, the sample was crushed, pelletized and sieved to obtain a 225-450 µm fraction. Finally, the pellets were carburized in a flow of 15 vol.,% CH_4/H_2 (50 $ml.min^{-1}$) as the temperature was increased from the room temperature to 200 °C at a heating rate of 10 °C.min^{-1}, and then from 200 to 590 °C at a rate of 1 °C.min^{-1}. The temperature was kept at 590 °C for 2 hrs.

The second wet impregnation was used to introduce promoters. In this step, a solution containing $Pt(NH_3)_4(OH)_2$ or copper (II) acetate monohydrate precursors were used following the procedure described above. The Pt and Cu metal loading in the obtained catalysts were 4 and 20 wt%, respectively. The samples were designated as X Pt-Y Mo_2C-Z where index X designates the Pt loading in wt%, index Y designates the Mo_2C loading in wt% and index Z designates the type of alumina support E- (η-Al_2O_3) and G– (γ-Al_2O_3).

2.3 Catalyst characterization

The characterisation techniques are described in the supplementary information.

2.4 Catalyst activity measurements

Prior to the catalytic tests, the catalysts were pre-treated in a flow of 15% CH_4/H_2 at a flow rate of 100 mL min^{-1} at 590 °C for 2 h with a heating rate 10 °C min^{-1}. In these experiments, 100 mg of catalyst (fraction size: 250-425 µm) was loaded in a fixed-bed reactor made of stainless steel (6 mm OD). The catalyst was placed between two plugs of quartz wool. A mixture of CO, CO_2, H_2, and helium was mixed with the corresponding water amount in order to achieve the desired feed gas composition of 11 vol.% CO, 43 vol.% H_2 and 6 vol.% CO_2, 21 vol.% H_2O, balance - He with a SV of 125,000 h^{-1}. The liquid flow was controlled with a high-performance liquid pump. The products were analyzed by an in-line Perkin Elmer 500 GC equipped with a Hayesep column, thermal conductivity Detector (TCD) and a flame ionization detector (FID).

3.Results

3.1. Catalyst characterization

3.1.1. XRD analysis

Figure 1a, shows the XRD patterns of the η-Al_2O_3, Mo_2C, 33 Mo_2C-E, 50 Mo_2C-E and 66 Mo_2C-E catalysts. The XRD patterns of the η-alumina support and a bulk molybdenum carbide catalyst are shown for comparison. The alumina support shows the diffraction peaks corresponding to η-Al_2O_3 (JCDD 04-0875). After exposure to air, the Mo_2C phase was oxidized to monoclinic MoO_2 (JCPDS:32-0671) [30]. The appearance of the monoclinic MoO_2 phase can be explained as follows. After carburization process in the CH_4/H_2 mixture, the molybdenum oxide species were fully converted into β-Mo_2C [9]. Afterwards, β-Mo_2C was converted into MoO_2 by a spontaneous oxidation reaction in the air as seen in Equation 1 and 2 with the final phase composition confirmed by the XRD results [4].

$$Mo_2C\,(s) + \ 3O_2(g) \leftrightarrow \ 2MoO_2(s) + CO_2(g) \quad (1)$$

$$Mo_2C\,(s) + \ \frac{5}{2}O_2(g) \leftrightarrow \ 2MoO_2(s) + CO(g) \quad (2)$$

The corresponding diffraction lines of MoO_2, especially those at 2θ= 26.12, 37.11 and 53.58° appeared in both of the studied molybdenum catalysts. The intensity of these lines increased as the molybdenum loading increased from 33 to 66% on η-Al_2O_3 support.

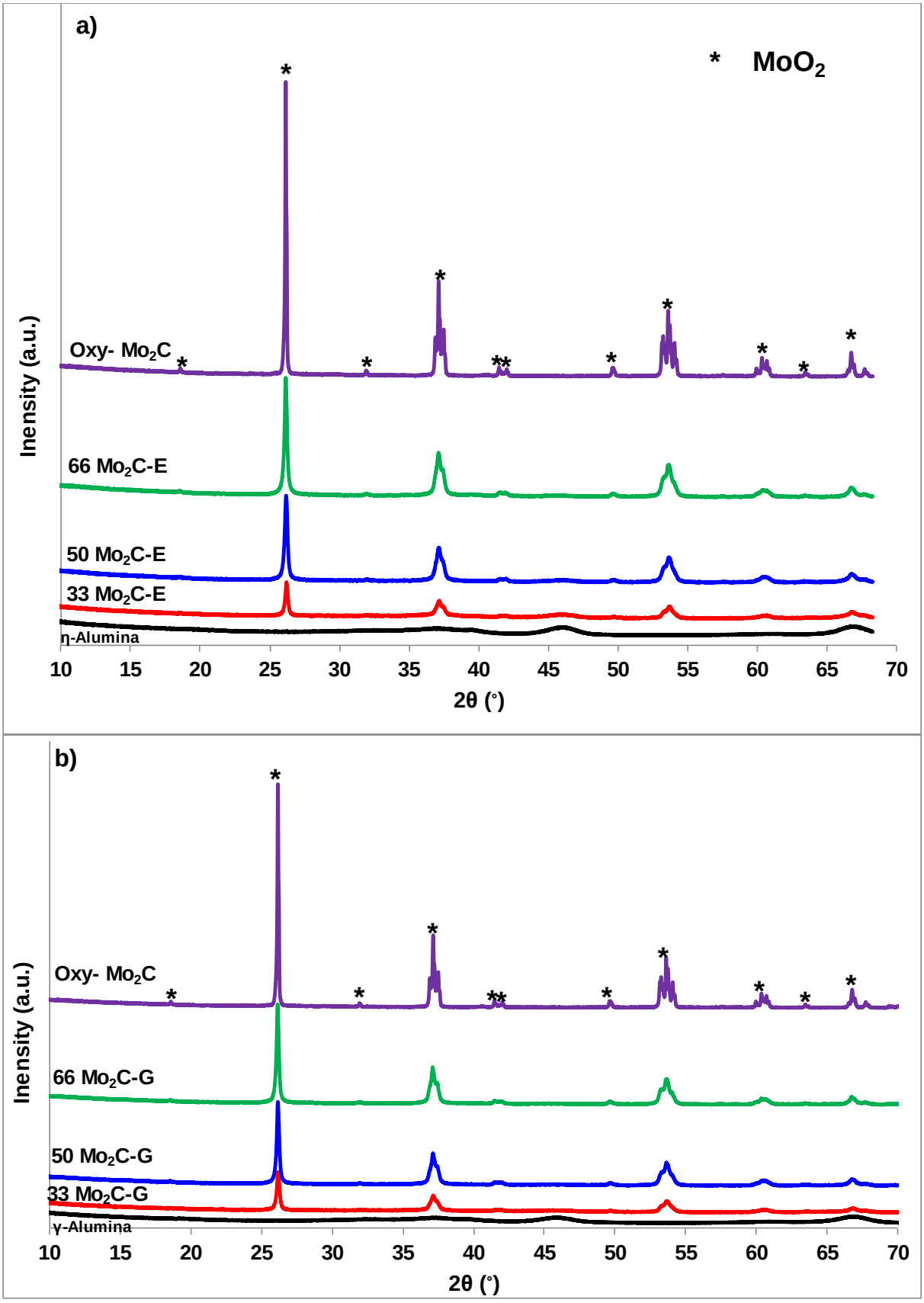

Figure 1: XRD patterns of a) η-Al_2O_3, Oxy-Mo_2C (passivated Mo_2C), 33 Mo_2C-E, 50 Mo_2C-E and 66 Mo_2C-E; b) γ-Al_2O_3, Mo_2C, 33 Mo_2C-G, 50 Mo_2C-G and 66 Mo_2C-G.

Figure 1b shows the XRD patterns of the γ-Al_2O_3, Mo_2C, 33 Mo_2C-G, 50 Mo_2C-G and 66 Mo_2C-G catalysts. The XRD patterns of the γ-alumina support and a bulk molybdenum carbide catalyst are shown for comparison. The pure alumina support showed the diffraction peaks corresponding to the γ-Al_2O_3 phase (JCDD 10-0425). Once again the bulk Mo-containing catalyst showed monoclinic MoO_2 phase (JCPDS:32-0671) [30]. It is obvious that three of these diffraction lines (2θ= 26.12, 37.11 and 53.58°) appeared in the alumina supported Mo_2C catalysts and these diffraction lines increased in intensity as the molybdenum loading increased from 33 to 66 wt.%. From a previous work [21], the pore volume of η-Al_2O_3 and γ-Al_2O_3 were 0.5 and 0.35 $cm^3.g^{-1}$, respectively, which suggest a higher Mo_2C dispersion on η-Al_2O_3 than that of γ-Al_2O_3.

Table 1 shows the surface area of the pure supports along with the Mo_2C loaded on η-Al_2O_3 or γ-Al_2O_3 support. The BET surface areas of the highest loading Mo_2C on η-Al_2O_3 and γ-Al_2O_3 supports are 100 and 79 $m^2.g^{-1}$, respectively. The higher surface area in case of η-Al_2O_3 is due to its higher pore volume than that of γ-Al_2O_3 resulting from a higher Mo_2C dispersion. It is obvious that the surface area decreased with increasing the Mo_2C loading in both η-Al_2O_3 and γ-Al_2O_3 supports by 58 and 95 $m^2.g^{-1}$, respectively, while the pore volume decreased by approximately 0.05 $cm^3.g^{-1}$. This decrease in the surface area and pore volume suggested that Mo_2C are filling the pores or deposits on alumina supports.

Table 1: Surface area of the supports along with the metals loaded on Mo_2C/η-Al_2O_3, Mo_2C/γ-Al_2O_3 or Mo_2C catalysts.

Catalyst Abbreviation	S_{BET} ($m^2.g^{-1}$)	Pore volume ($cm^3.g^{-1}$)
33 Mo_2C-E	159	0.27
50 Mo_2C-E	130	0.24
66 Mo_2C-E	101	0.21
33 Mo_2C-G	175	0.18
50 Mo_2C-G	131	0.16
66 Mo_2C-G	79	0.13
4 Pt-66 Mo_2C-E	63	0.10
4 Pt-66 Mo_2C-G	37	0.06
20 Cu-66 Mo_2C-E	51	0.11
20 Cu-66 Mo_2C-G	52	0.07
20 Cu -Mo_2C	21	0.03
4 Pt-Mo_2C	61	0.10
Mo_2C	70	0.11

Figure 2 shows the XRD patterns of Pt or Cu modified Mo_2C or Mo_2C/Al_2O_3 supports. Again, the main three diffraction lines appeared in all of the prepared catalysts. 4 Pt-66 Mo_2C-E and 4 Pt-66 Mo_2C-G catalysts showed two extra diffraction peaks at 2θ= 39.61 and 46.42° which corresponding to the reflections (111),(200), respectively, of face-centred cubic (fcc) structure of platinum metal [31, 32] (JCPDS PDF 04-0802). The appearance of platinum diffraction peaks on those two previous supports confirmed a Pt deposition with relatively large particle size over the alumina surface compared with 4 Pt-Mo_2C catalyst which showed no appearance of Pt diffraction peaks; this is may be due to the synergetic effect between Pt and Mo_2C [14, 33]. In copper modified catalysts, Cu metal diffraction lines (JCPDS 04-0836) appeared at 2θ= 43.60 and 50.81° corresponding to (111) and (200), respectively. The 20 Cu-Mo_2C catalyst showed an extra diffraction line at 2θ= 39.51° corresponding to copper oxide phase [34].

Table 1 shows the surface area of the Cu or Pt-modified Mo_2C or Mo_2C/Al_2O_3 supports. Interestingly, the surface area of the pure Mo_2C decreased on loading previously, it was 4 wt% from 70 to 61 $m^2.g^{-1}$, and the pore volume remained relatively constant, confirming the synergetic effect between Pt and Mo_2C [14, 33]. The same effect occurred with 20 Cu-Mo_2C as the surface area decreased to 21 $m^2.g^{-1}$. Conversely, the surface area of all other catalysts dramatically decreased with loading 4 wt% Pt. For instance, the surface area of 66 Mo_2C-E and 66 Mo_2C-G catalysts were 101 and 79 $m^2.g^{-1}$, respectively and decreased by loading Pt to 63 and 37 $m^2.g^{-1}$, respectively. The same effect occurred upon loading 20 wt% Cu over these two catalysts as the surface area decreased to 51 and 52 $m^2.g^{-1}$, respectively.

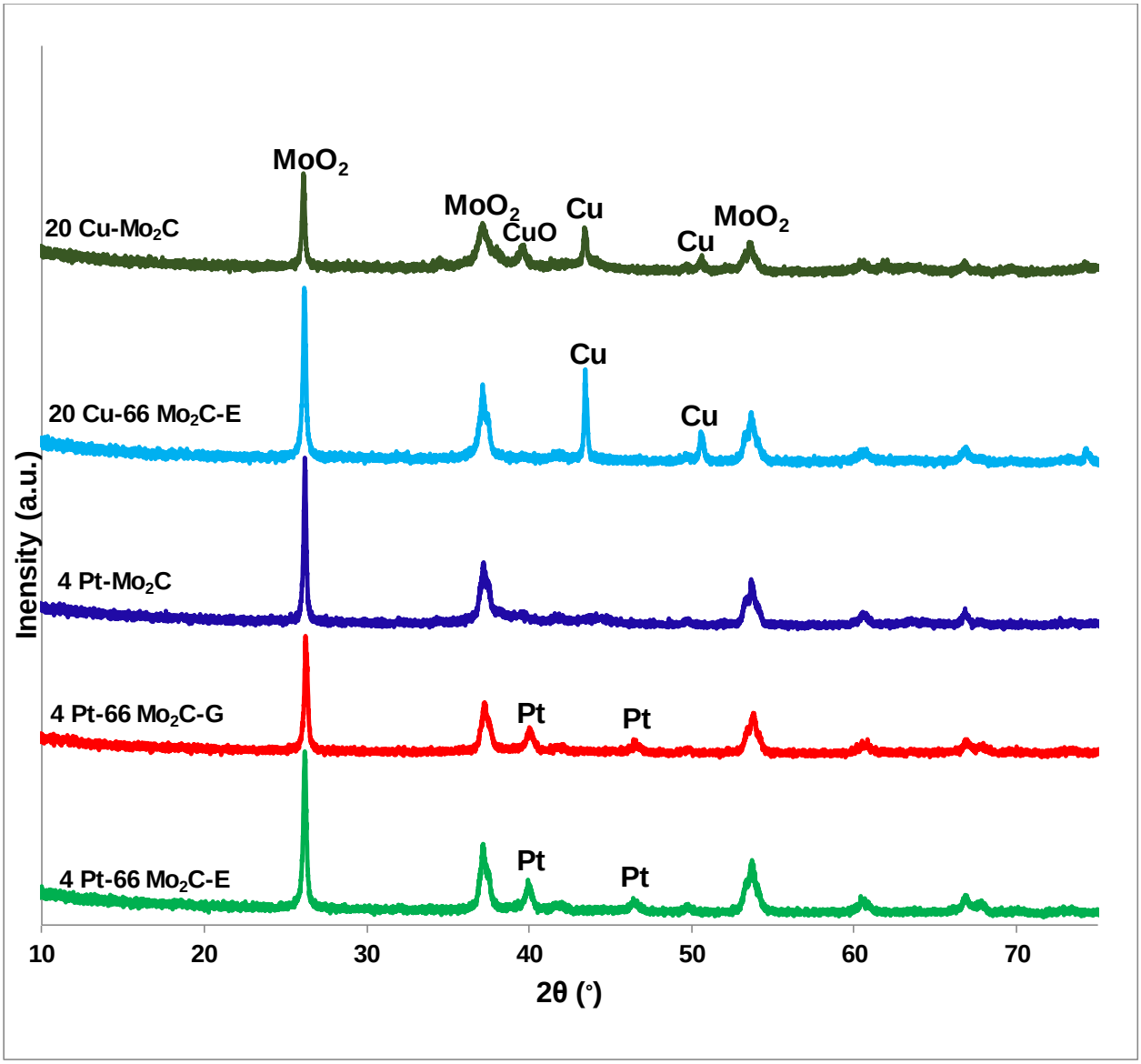

Figure 2: XRD patterns of 4 Pt-66 Mo_2C-G, 4 Pt-66 Mo_2C-E, 4 Pt-Mo_2C, 20 Cu-66 Mo_2C-E and 20 Cu -Mo_2C.

3.1.2. H_2-TPR analysis

Figure 3 shows the H_2-TPR profiles of 4 Pt-66 Mo_2C-G, 4 Pt-66 Mo_2C-E, 4 Pt-Mo_2C and 20 Cu-Mo_2C catalysts as each catalyst showed one reduction peak at 20, 9, 88 and 280 °C, respectively. It is well known that using the reducible supports is more active than that of irreducible supports in WGSR [4]. It is apparent that all the Pt-containing catalysts reduced much easier than that of Cu containing catalyst. Among the Pt-containing catalysts, 4 Pt-Mo_2C

catalyst showed the largest reduction peak which should facilitate the oxidation-reduction cycle and consequently improve the catalytic activity of the catalyst followed by the reduction peak of 4 Pt-66 Mo_2C-E catalyst. Using the same molybdenum precursor and carburization procedures, pure Mo_2C was prepared by Wang et al.[9] and Schweitzer et al.[4] and H_2-TPR characterization showed a single reduction peak at 250 °C. In our work, loading 4% Pt enhanced the reduction process where the reduction peak shifted to a lower temperature at 88 °C compared to the literature.

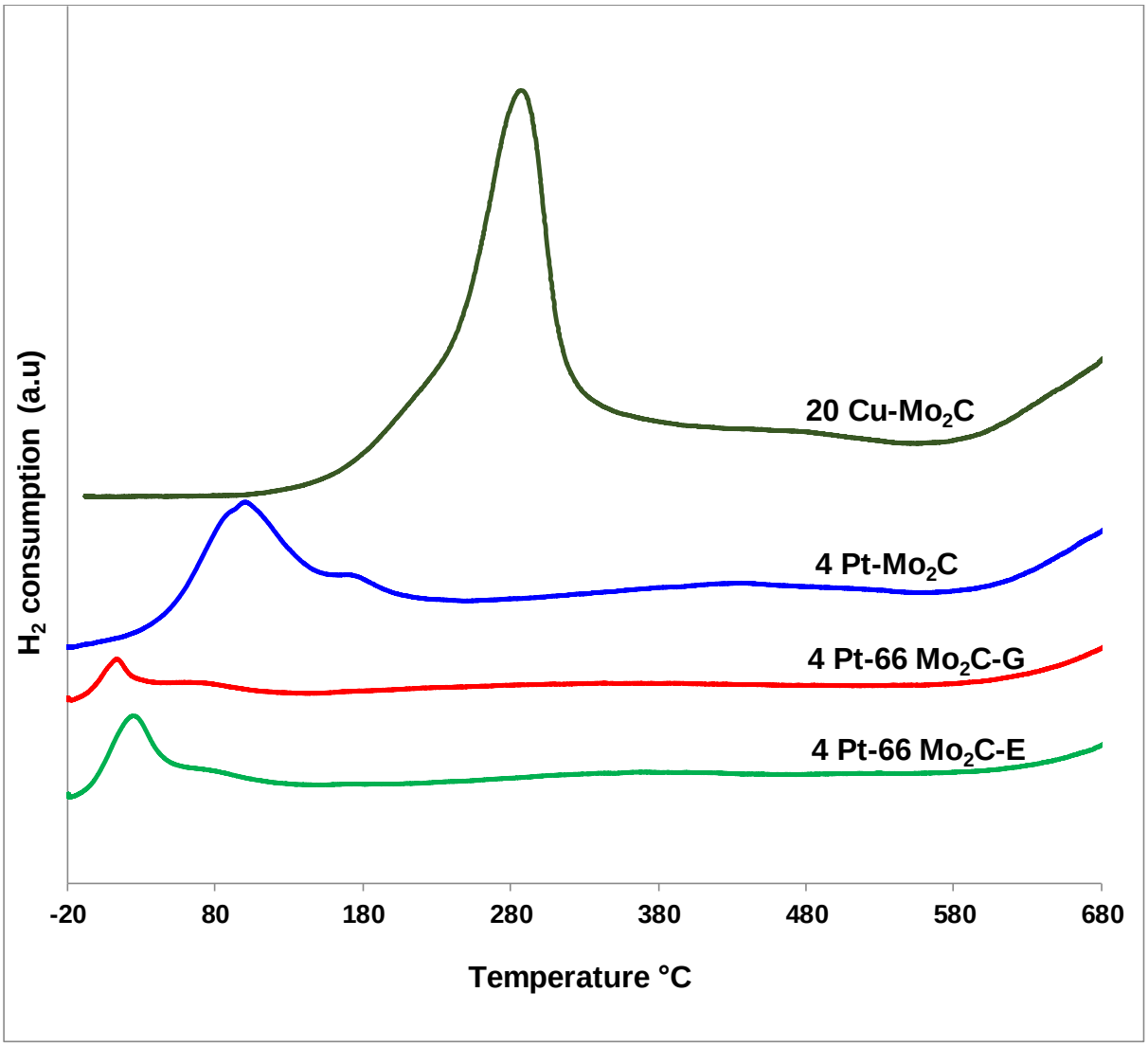

Figure 3: H_2-TPR profiles of 4 Pt-66 Mo_2C-G, 4 Pt-66 Mo_2C-E, 4 Pt-Mo_2C and 20 Cu -Mo_2C.

3.1.3. SEM-EDX analysis

Figure 4 shows the SEM images of 4 Pt-66 Mo_2C-E, 4 Pt-66 Mo_2C-G, 4 Pt-Mo_2C, and 20 Cu -Mo_2C catalysts. The particles formed clusters in 4 Pt-66 Mo_2C-E, 4 Pt-66 Mo_2C-G, and 20 Cu -Mo_2C catalysts. While the catalyst 4 Pt-Mo_2C catalyst showed good particle size distribution. Moreover, the 4 Pt-Mo_2C catalyst showed smaller particle size than that of the original Mo_2C catalyst as seen in Figure 5.

Table 2 shows the EDX data of Mo_2C, 4 Pt-66 Mo_2C-E, 4 Pt-66 Mo_2C-G, 4 Pt-Mo_2C and 20 Cu -Mo_2C catalysts. EDX showed that 4 Pt-Mo_2C offered the best Pt particle size distribution by showing 4.3 wt% of Pt. While 4 Pt-66 Mo_2C-E and 4 Pt-66 Mo_2C-G catalysts showed Pt content around 5.5 % and this agrees with the SEM images that showed a cluster formation on the surface of these two catalysts. The copper loading in 20 Cu -Mo_2C was 20 wt%; EDX result showed 18.6% and this is may be due to the poor copper dispersion as shown by SEM images in Figure 4.

Table 2: EDX data of Pure Mo_2C, 4 Pt-66 Mo_2C-E, 4 Pt-66 Mo_2C-G, 4 Pt-Mo_2C and 20 Cu -Mo_2C.

	Pt (wt. %)	**Mo (wt. %)**	**O (wt. %)**	**Al (wt. %)**	**Cu (wt. %)**
Mo_2C	--	69.5	30.5	--	--
4 Pt-66 Mo_2C-E	5.1	52.0	35.3	7.5	--
4 Pt-66 Mo_2C-G	5.5	48.3	35.9	10.3	--
4 Pt-Mo_2C	4.3	64.6	31.1	--	--
20 Cu -Mo_2C	--	54.4	27.0	--	18.6

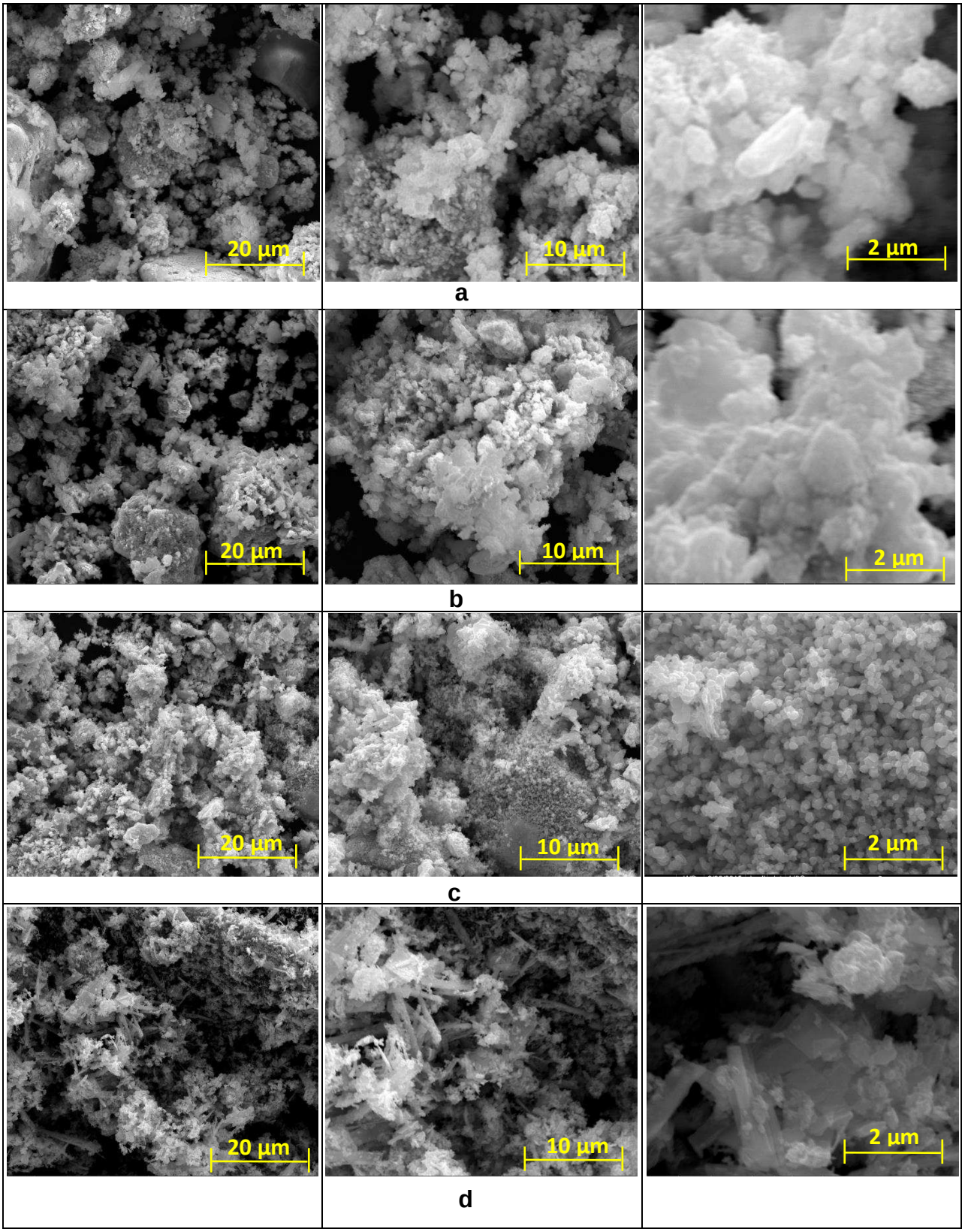

Figure 4: SEM images for a) 4 Pt-66 Mo_2C-E, b) 4 Pt-66 Mo_2C-G, c) 4 Pt-Mo_2C, and d) 20 Cu -Mo_2C at a different level of magnifications using ETD detector.

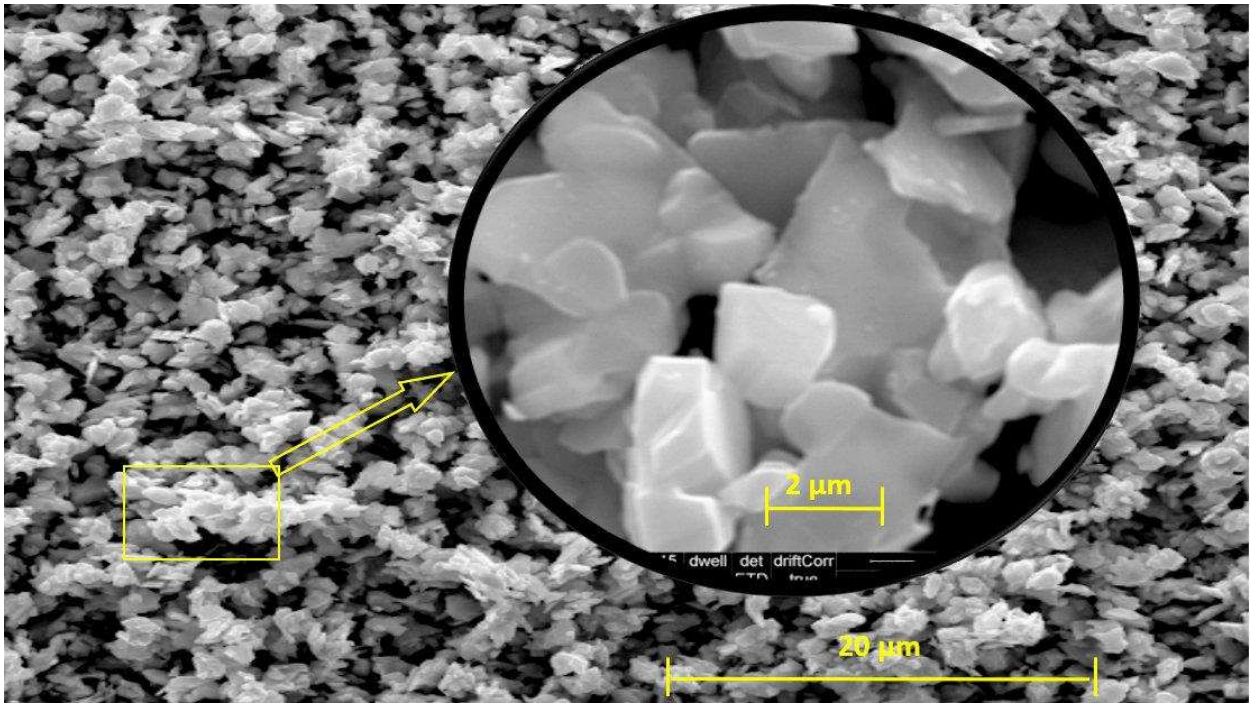

Figure 5: SEM image of the pure Mo_2C catalyst.

3.1.4. Understanding the catalyst structure using XPS analysis

To understand the catalyst structure and molybdenum carbide behaviour of 4 Pt-66 Mo_2C-G, 4 Pt-66 Mo_2C-E, XPS and XRD analyses were utilised. X-ray photoelectron spectra of the partially oxidised samples (left in air for short time) are presented in Figure 6. The Mo peak for the 4 Pt-66 Mo_2C-G sample shows the presence of Mo in three oxidation states; as Mo_2C, MoO_2 and MoO_3 in the molar ratio of 64:11:25, respectively. Figure 6b shows that Pt was present in the metallic form on the catalyst surface. Moreover, there is a small peak of Al which was also observed at the binding energy of around 120 eV and corresponded to the γ-Al_2O_3 support material. Interestingly, the survey spectrum showed Mo to Al mass ratio of 5.8, while the nominal sample composition provided the value of 2.2. A significantly higher relative amount of Mo observed on the surface-specific photoelectron spectroscopy indicates that the Mo compounds efficiently covered the surface of the γ-Al_2O_3 support. The Pt to Mo mass ratio was about 0.057 which agrees with the nominal ratio of 0.060.

Figure 6c shows the Mo 3d peak of the 4 Pt-66 Mo_2C-E catalyst, where three oxidation states of Mo can be observed in the molar ratio of 46:17:37 for Mo_2C, MoO_2 and MoO_3, respectively. The 4 Pt-66 Mo_2C-E sample compared to the 4 Pt-66 Mo_2C-G one shows a lower amount of Mo_2C and an increased MoO_3. In contrast to the 4 Pt-66 Mo_2C-G sample, the 4 Pt-66 Mo_2C-E sample Figure 6d shows the presence of Mo peak close to that for Pt, but no Al. The latter is surprising considering the nominal Al content of 30 wt%. However, considering that XPS is a very surface-specific method, the absence of Al on the spectra can be explained by full coverage of the η-Al_2O_3 support with Mo which is feasible considering high Mo content. The possibility of η-Al_2O_3 coverage is also supported by the very low Pt to Mo mass ratio observed of 0.006 for the 4 Pt-66 Mo_2C-E sample, while the nominal loading was 0.060. Thus, the possible interaction between Pt and Mo_2C which are the two active sites in WGSR in the case of 4 Pt-66 Mo_2C-E is shown in Scheme 1. On the other hand, 4 Pt-66 Mo_2C-G showed an interaction between Pt and γ-Al_2O_3 on the surface of the catalyst as shown in Figure 6 b and Scheme 1. Therefore, XPS results revealed that by using different acidic supports (η-Al_2O_3 and γ-Al_2O_3) in the catalyst composition, this led to different interaction because Pt in the catalyst was substantially below the Mo_2C surface as confirmed by the survey spectra and showed in Scheme 1 along with and synergetic effect between the two most active phases of Pt metal and Mo_2C which is greater in the case of 4 Pt-66 Mo_2C-E (η-Al_2O_3) catalyst than that of 4 Pt-66 Mo_2C-G (γ-Al_2O_3). We reported earlier that η-Al_2O_3 and γ-Al_2O_3 catalysts can be prepared from different precursors of aluminium nitrates and chloride, respectively [21]. The produced catalysts showed different surface morphology and acidity with η-Al_2O_3 showed higher acidity and better morphology than that of the γ-Al_2O_3 catalyst. η-Al_2O_3 showed a total acidity and the acid site density of 8.56 $x10^{20}$ (sites.g^{-1}) and 3.8 $x10^{18}$ (sites.m^{-2}), while γ-Al_2O_3 showed values of 6.91 $x10^{20}$ (sites.g^{-1}) and 2.5 $x10^{18}$ (sites.m^{-2}), respectively. Furthermore, η-Al_2O_3 offered a larger pore volume of 0.5 $cm^3.g^{-1}$

compared with that of γ-Al_2O_3 of 0.35 $cm^3.g^{-1}$. The superior morphology and acidity of η-Al_2O_3 offered a better dispersion of Pt with a close interaction with Mo_2C.

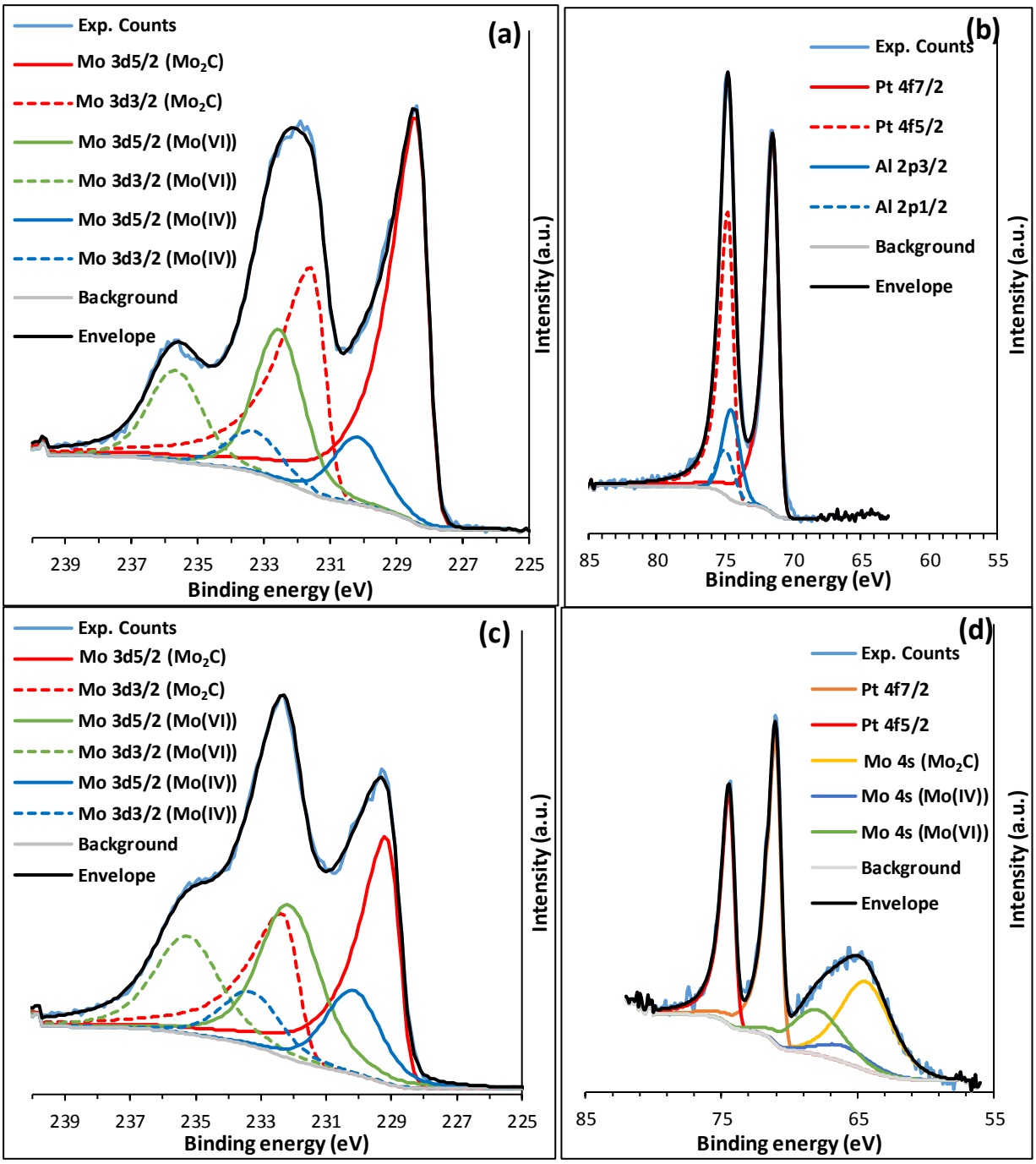

Figure 6: X-ray photoelectron spectra for the 4 Pt-66 Mo_2C-G sample (a) Mo 3d, (b) Pt 4f peaks and for the 4 Pt-66 Mo_2C-E sample, (c) Mo 3d and (d) Pt 4f peaks.

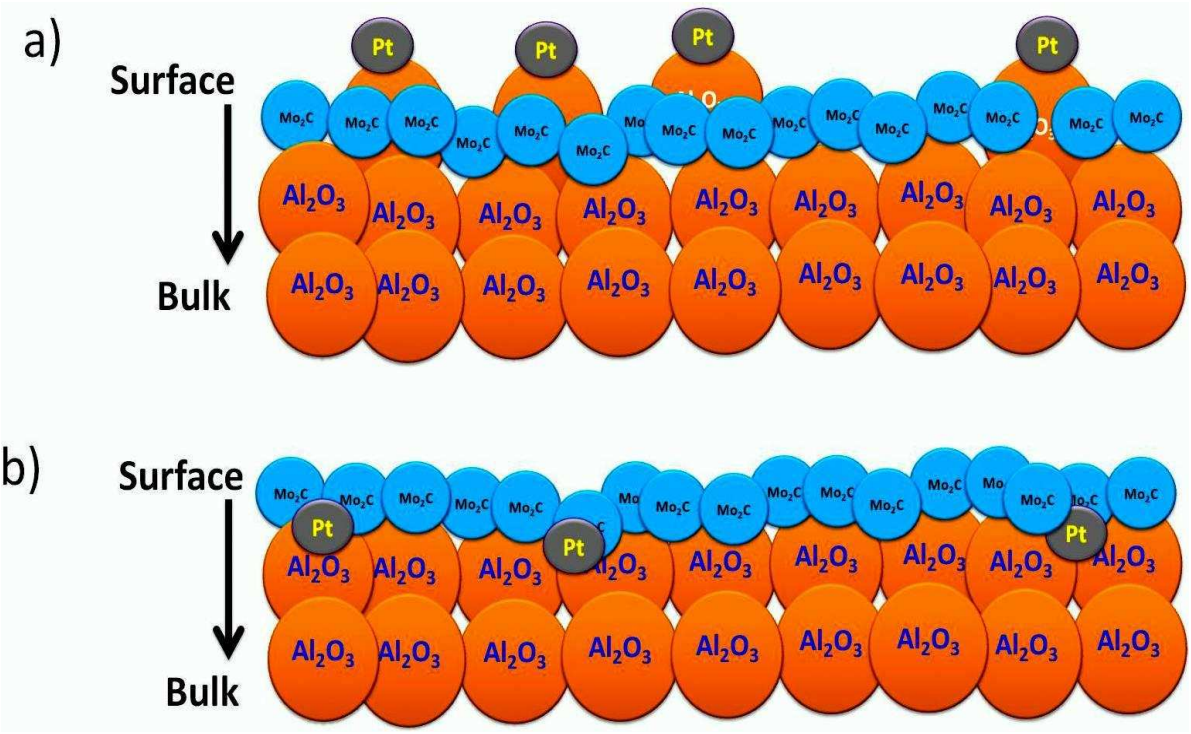

Scheme 1: Schematic representation of the structure of 4 Pt-66 Mo_2C-G (a) and 4 Pt-66 Mo_2C-E (b) catalysts derived from the XPS results.

Namiki et al.[35] used in-situ XPS and DRIFTS techniques to study the mechanism of WGSR over Mo_2C catalyst and found that the WGSR on the carburised Mo_2C/Al_2O_3 preceded the redox route based on the dissociation of H_2O and CO. Therefore, a good WGSR catalyst indicates a facile reduction/oxidation cycle between the two phases of Mo_2C and MoOx under reaction conditions, thus we investigated the nature of the re-oxidation of Mo_2C phase. The in-situ XRD study shown in Figure S1 (supplementary) demonstrate that the carburized catalyst then left in air for a short time (4 Pt-66 Mo_2C-E, reduced) has Pt, Mo_2C and MoO_3 phases. Even gentle heating to 100 ^oC in the air (4 Pt-66 Mo_2C-E, fresh) results in a significant decrease in the relative intensity of the Mo_2C reflections and increase in MoO_2 indicating the quick oxidation of the carbide.

4. Catalytic activity

It was reported that Mo_2C showed higher catalytic activity than that of commercial catalyst for WGSR [4]. Herein, we used different supports with copper or platinum loadings as described in Table 1. Figure 7 a shows the catalytic activity profiles for WGSR over Mo_2C, 33 Mo_2C-E, 50 Mo_2C-E and 66 Mo_2C-E catalyst with different Mo_2C loadings over the temperature range 180-300 °C. The conversion increases with increasing either the reaction temperature or the Mo_2C loading, which can be explained as Mo_2C is the only active site for the WGSR and is responsible for the dissociation of water to react with the CO species. The same trend is noticed in the 33 Mo_2C-G, 50 Mo_2C-G, 66 Mo_2C-G and Mo_2C catalysts as shown in Figure 7b but with less catalytic activity at the same Mo_2C loading and different support. For instance, the conversion at 300 °C for 66 Mo_2C-E and 66 Mo_2C-G are 27.17 and 24.1, respectively. The higher activity in the presence of η-Al_2O_3 support can be attributed to the synergetic effect between Pt and Mo_2C as shown from the XPS results in Figure 6 and Scheme 1 along with the higher pore volume of 0.5 for η-Al_2O_3 and 0.35 for γ-Al_2O_3. Although Mo_2C, 66 Mo_2C-E and 66 Mo_2C-G showed the highest catalytic activity in the previous series of catalysts, those catalysts still require further promotion to achieve better catalytic activity and stability during the WGSR. Thus, 4 wt.% Pt and 20 wt.% Cu metals were added to that catalyst where the final prepared catalysts designated as 4 Pt-Mo_2C, 4 Pt-66 Mo_2C-E, 4 Pt-66 Mo_2C-G, 20 Cu-Mo_2C, 20 Cu-66 Mo_2C-E and 20 Cu-66 Mo_2C-G.

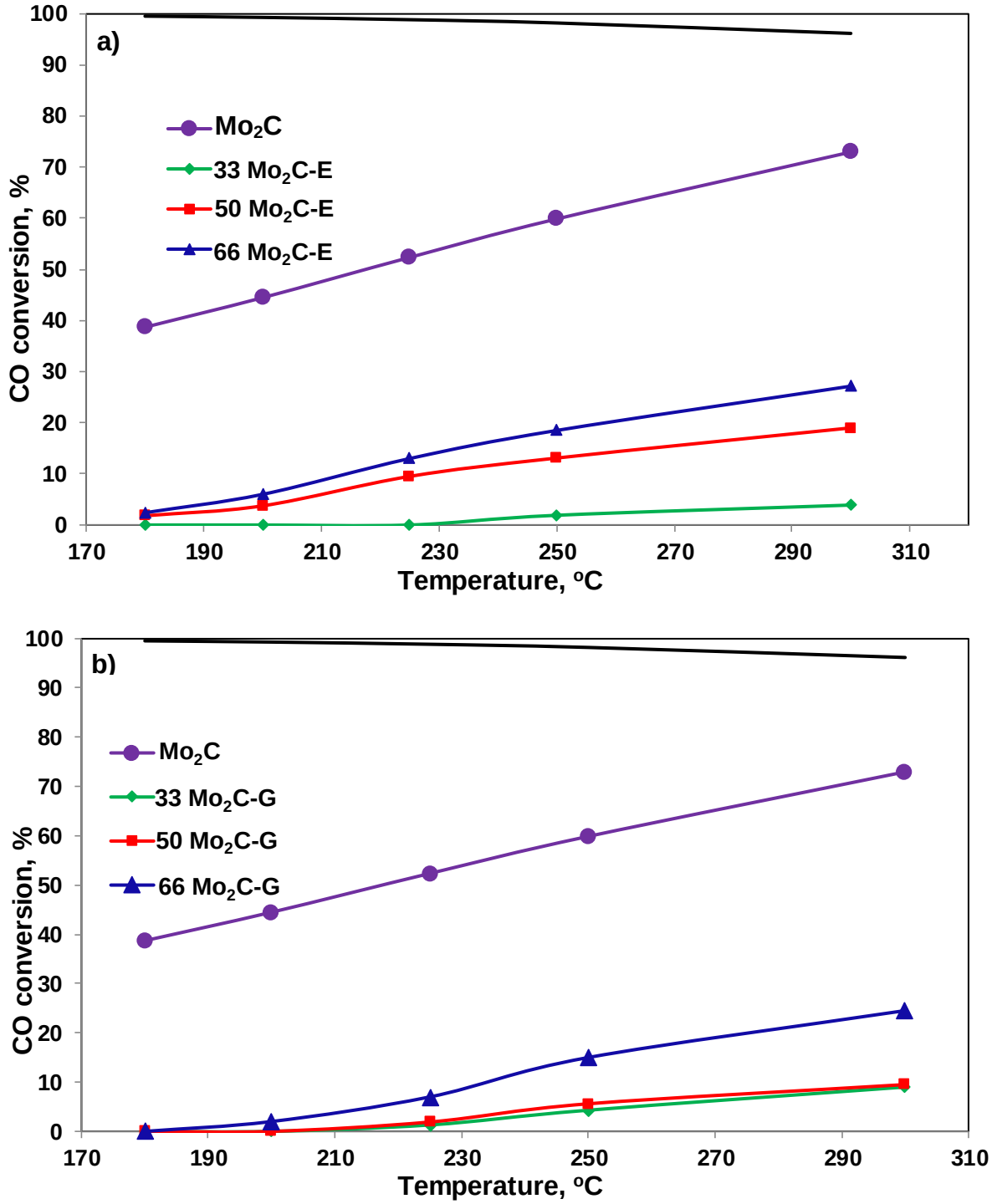

Figure 7: Catalytic activity profiles for WGSR over a) Mo_2C, 33 Mo_2C-E, 50 Mo_2C-E and 66 Mo_2C-E; b) Mo_2C, 33 Mo_2C-G, 50 Mo_2C-G and 66 Mo_2C-G along with the equilibrium line in black colour. Reaction conditions: temperature, 180-300 °C; SV ~ 125,000 h^{-1}. 11% CO, 43% H_2, 6% CO_2, 21% H_2O, and balance He.

Figure 8 shows the catalytic activity for WGSR over different catalysts of 4 Pt-Mo_2C, 4 Pt-66 Mo_2C-E, Mo_2C, 4 Pt-66 Mo_2C-G, 20 Cu -Mo_2C, 20 Cu-66 Mo_2C-E, 20 Cu-66 Mo_2C-G along with the commercial CuZnAl catalysts. In all catalysts, the CO conversion increased with increasing the reaction temperature. All the copper catalysts loaded Mo_2C or Mo_2C-alumina support exhibit low activity at reaction temperatures below 250 °C and have lower conversion than the Pt-based catalysts. For instance, at a reaction temperature of 300 ºC, 20 Cu -Mo_2C and 4 Pt-Mo_2C have catalytic conversions of 58 and 81.9 %, respectively. Such differences can be attributed to the active site in metal/Mo_2C catalysts is bi-functional for WGSR as proved by Sabnis et al.[20]. Moreover, the reducibility of the catalyst can play a big role in the catalytic activity, as confirmed by the TPR results, where the reduction temperature for 20 Cu -Mo_2C was 280 °C whereas for 4 Pt-Mo_2C is 88 °C.

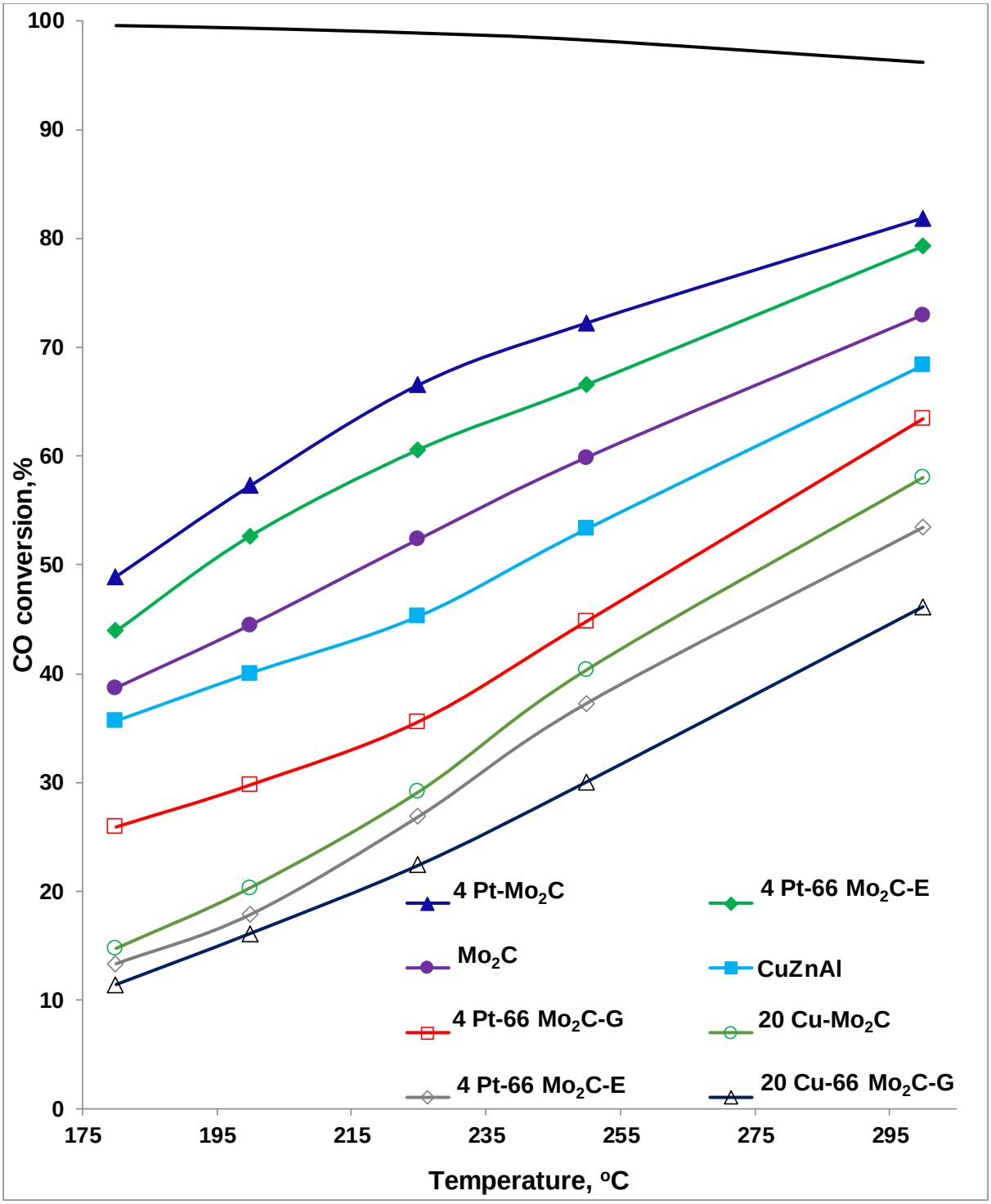

Figure 8: Catalytic activity profiles for WGSR over 4 Pt-Mo_2C, 4 Pt-66 Mo_2C-E, Mo_2C, 4 Pt-66 Mo_2C-G, 20 Cu-Mo_2C, 20 Cu-66 Mo_2C-E, 20 Cu-66 Mo_2C-G and CuZnAl catalysts along with the equilibrium line in black colour. Reaction conditions: temperature, 180-300 °C; SV ~ 125,000 h^{-1}. 11% CO, 43% H_2, 6% CO_2, 21% H_2O, and balance He.

For the catalyst to meet the commercialization requirements, it should offer good stability behaviour during the operating conditions. Figure 9 shows a comparison of the stability of Mo_2C, 4 Pt-66 Mo_2C-E and 4 Pt-Mo_2C at a reaction temperature of 250°C for 85 h. The catalytic activity of 4 Pt-66 Mo_2C-E and 4 Pt-Mo_2C is similar at time zero on stream but with time on stream, the CO conversion over 4 Pt-66 Mo_2C-E decreased from 68 to 43% after 30 h then stabilised for the next 55 h, while 4 Pt-Mo_2C was stable over the reaction time which is in agreement with the results of Yan et al.[14].

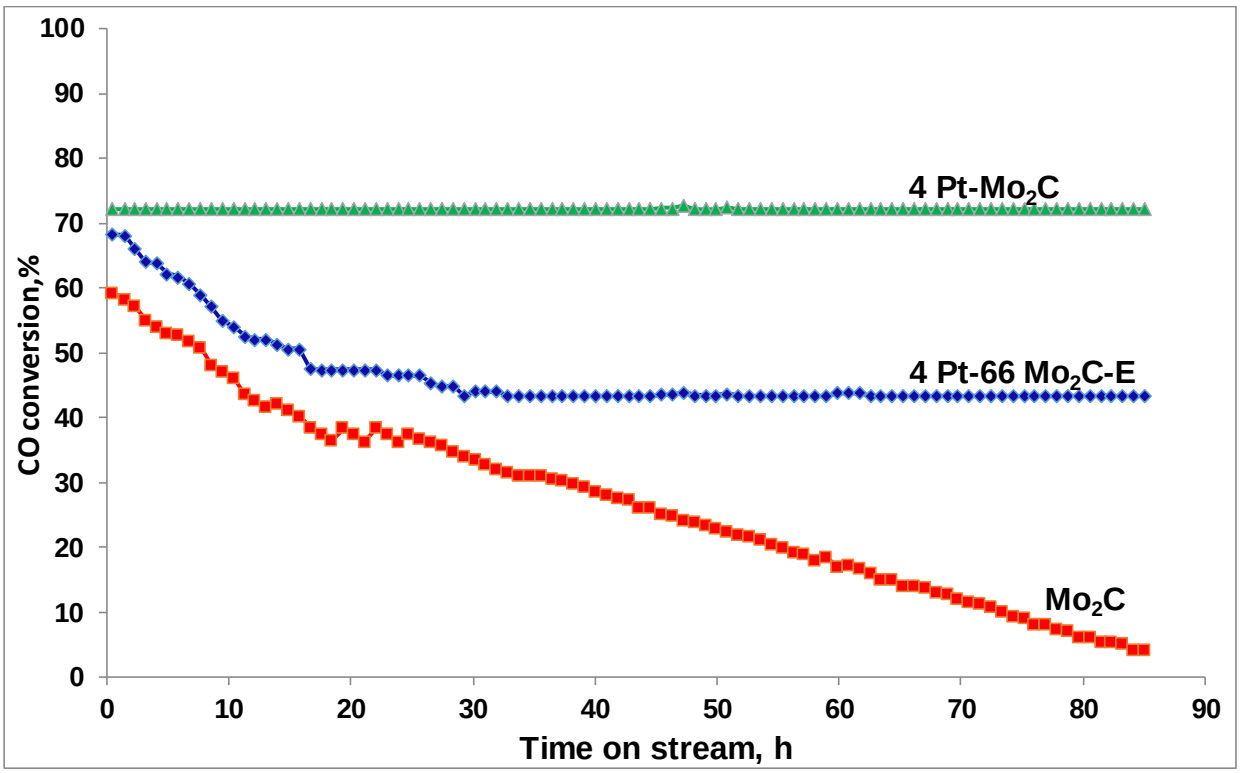

Figure 9: Comparison of the stability of Mo_2C, 4 Pt-66 Mo_2C-E and 4 Pt-Mo_2C. Reaction conditions: temperature, 250°C for 85 hr; SV ~ 125,000 h^{-1}. 11% CO, 43% H_2, 6% CO_2, 21% H_2O, and balance He.

Compared with the literature, our results show 4-5 times higher activity with the $T_{50\%}$ for Pt-Mo_2C was 180℃ which is lower than in previous research work performed over the Pt/CeO_2 catalyst, which showed the $T_{50\%}$ value of 400℃ [36]. On the addition of Pt, the stability experiments showed no decrease in the catalyst activity over 85 hours at 250 °C.

5. Conclusion

Herein different Pt and Cu based catalysts at different supports (Mo_2C, 4 Pt-66 Mo_2C-E and 4 Pt-66 Mo_2C-G) were studied for low-temperature water gas shift reaction. The prepared catalysts were used in WGSR and compared with the commercial catalyst using a real feed composition mixture from the reformer (11 % CO, 43 % H_2, 6% CO_2, 21 % H_2O). It was found that the 4 Pt-Mo_2C catalyst has the highest activity and the most stable catalyst over 85 hours at 250 °C. XPS results revealed that by using different acidic supports (η-Al_2O_3 and γ-Al_2O_3) led to different interaction and synergetic effect between the two most active phases of Pt metal and Mo_2C.

Acknowledgement

The financial support from the FP7-NMP project BIOGO (grant: 604296) is kindly acknowledged.

Conflict of Interest Statement: The authors declare no conflict of interest.

6. References

[1] C. Ratnasamy, J.P. Wagner, Catalysis Reviews, 51 (2009) 325-440.
[2] R. Burch, Physical Chemistry Chemical Physics, 8 (2006) 5483-5500.
[3] P. Sangeetha, K. Shanthi, K.S.R. Rao, B. Viswanathan, P. Selvam, Applied Catalysis A: General, 353 (2009) 160-165.
[4] N.M. Schweitzer, J.A. Schaidle, O.K. Ezekoye, X. Pan, S. Linic, L.T. Thompson, Journal of the American Chemical Society, 133 (2011) 2378-2381.
[5] C. Wheeler, A. Jhalani, E.J. Klein, S. Tummala, L.D. Schmidt, Journal of Catalysis, 223 (2004) 191-199.
[6] S.Y. Choung, M. Ferrandon, T. Krause, Catalysis Today, 99 (2005) 257-262.
[7] W.D. Williams, L. Bollmann, J.T. Miller, W.N. Delgass, F.H. Ribeiro, Applied Catalysis B: Environmental, 125 (2012) 206-214.
[8] K.D. Sabnis, Y. Cui, M.C. Akatay, M. Shekhar, W.-S. Lee, J.T. Miller, W.N. Delgass, F.H. Ribeiro, Journal of Catalysis, 331 (2015) 162-171.
[9] G. Wang, J.A. Schaidle, M.B. Katz, Y. Li, X. Pan, L.T. Thompson, Journal of Catalysis, 304 (2013) 92-99.
[10] M.K. Gnanamani, G. Jacobs, W.D. Shafer, D.E. Sparks, S. Hopps, G.A. Thomas, B.H. Davis, Topics in Catalysis, 57 (2014) 612-618.
[11] D.J. Moon, J.W. Ryu, Catalysis Letters, 92 (2004) 17-24.
[12] A.R. Dubrovskii, S.A. Kuznetsov, E.V. Rebrov, J.C. Schouten, Russian Journal of General Chemistry, 82 (2012) 2070-2078.
[13] A.R. Dubrovskii, S.A. Kuznetsov, E.V. Rebrov, J.C. Schouten, Russian Journal of Applied Chemistry, 87 (2014) 601-607.
[14] Z. Yan, H. Wang, M. Zhang, Z. Jiang, T. Jiang, J. Xie, Electrochimica Acta, 95 (2013) 218-224.
[15] E.V. Rebrov, A. Berenguer-Murcia, B.F.G. Johnson, J.C. Schouten, Catalysis Today, 138 (2008) 210-215.
[16] E.V. Rebrov, S.A. Kuznetsov, M.H.J.M. de Croon, J.C. Schouten, Catalysis Today, 125 (2007) 88-96.
[17] S.A. Kuznetsov, A.R. Dubrovskiy, E.V. Rebrov, J.C. Schouten, Zeitschrift für Naturforschung A, 62 (2007) 647-654.
[18] A.R. Dubrovskii, S.A. Kuznetsov, E.V. Rebrov, J.C. Schouten, Kinetics and Catalysis, 49 (2008) 594-598.
[19] A.R. Dubrovskiy, E.V. Rebrov, S.A. Kuznetsov, J.C. Schouten, Catalysis Today, 147, Supplement (2009) S198-S203.
[20] K. Sabnis, M. Shekhar, J. Lu, M.C. Akatay, J. Elam, J.T. Miller, W.N. Delgass, F.H. Ribeiro, in: AIChE 2012 - 2012 AIChE Annual Meeting, Conference Proceedings, 2012.
[21] A.I. Osman, J.K. Abu-Dahrieh, D.W. Rooney, S.A. Halawy, M.A. Mohamed, A. Abdelkader, Applied Catalysis B: Environmental, 127 (2012) 307-315.
[22] A.I. Osman, J.K. Abu-Dahrieh, Catalysis Letters, 148 (2018) 1236-1245.
[23] H. Pennemann, M. Dobra, M. Wichert, G. Kolb, Chemical Engineering & Technology, 36 (2013) 1033-1041.

[24] A.I. Osman, J.K. Abu-Dahrieh, F. Laffir, T. Curtin, J.M. Thompson, D.W. Rooney, Applied Catalysis B: Environmental, 187 (2016) 408-418.
[25] A.I. Osman, J.K. Abu-Dahrieh, M. McLaren, F. Laffir, D.W. Rooney, ChemistrySelect, 3 (2018) 1545-1550.
[26] A.I. Osman, J. Meudal, F. Laffir, J. Thompson, D. Rooney, Applied Catalysis B: Environmental, 212 (2017) 68-79.
[27] A.I. Osman, J.K. Abu-Dahrieh, D.W. Rooney, J. Thompson, S.A. Halawy, M.A. Mohamed, Journal of Chemical Technology & Biotechnology, 92 (2017) 2952-2962.
[28] A.I. Osman, J.K. Abu-Dahrieh, M. McLaren, F. Laffir, P. Nockemann, D. Rooney, Nature Scientific Reports, 7 (2017) 3593.
[29] A.I. Osman, J.K. Abu-Dahrieh, A. Abdelkader, N.M. Hassan, F. Laffir, M. McLaren, D. Rooney, The Journal of Physical Chemistry C, 121 (2017) 25018-25032.
[30] S. Yoon, A. Manthiram, Journal of Materials Chemistry, 21 (2011) 4082-4085.
[31] T. Hyde, Platin Met Rev, 52 (2008) 129-130.
[32] M.A. Shah, Scientia Iranica, 19 (2012) 964-966.
[33] K. Zhang, W. Yang, C. Ma, Y. Wang, C.W. Sun, Y.J. Chen, P. Duchesne, J.G. Zhou, J. Wang, Y.F. Hu, M.N. Banis, P. Zhang, F. Li, J.Q. Li, L.Q. Chen, Npg Asia Materials, 7 (2015) 1-10.
[34] S. Elzey, J. Baltrusaitis, S. Bian, V.H. Grassian, Journal of Materials Chemistry, 21 (2011) 3162-3169.
[35] T. Namiki, S. Yamashita, H. Tominaga, M. Nagai, Applied Catalysis A: General, 398 (2011) 155-160.
[36] C. Wheeler, A. Jhalani, E.J. Klein, S. Tummala, Journal of catalysis, (2004).